IEEE Access
Multidisciplinary | Rapid Review | Open Access Journal

Received July 2, 2019, accepted July 17, 2019, date of publication August 5, 2019, date of current version November 4, 2019.

Digital Object Identifier 10.1109/ACCESS.2019.2933154

Design of Substrate Integrated Gap Waveguide and Their Transitions to Microstrip Line, for Millimeter-Wave Applications

JING ZHANG, (Student Member, IEEE), XIUPU ZHANG, (Senior Member, IEEE), AND AHMED A. KISHK, (Fellow, IEEE)

Department of Electrical and Computer Engineering, Concordia University, Montreal, QC H3G1M8, Canada

Corresponding author: Jing Zhang (z_jin25@encs.concordia.ca)

This work was supported by the Quebec FQRNT Project in Broadband Photonic Devices.

ABSTRACT This paper offers an approximate, but very convenient and accurate, manner to find the desired strip width for substrate integrated gap waveguide (SIGW) with a given characteristic impedance and the conductor and dielectric attenuation constants, without any complicated manual calculations or time-consuming full-wave simulation and optimization iterations. Moreover, the investigation of the transition between SIGW and microstrip lines will prove that an additional transition structure, such as a conventional microstrip taper, is not required any more at millimeter-wave frequencies for the desired transmission performance. This is a useful feature in circuit design and compactness. Both of the above works will be of great help to realize future feeding networks for SIGW antenna arrays or other types of cost-effective SIGW passive components at high frequencies. Two SIGW prototypes, working at Ka and V bands, are fabricated and offer experimental verifications, which present good agreement with the simulation results.

INDEX TERMS Gap waveguide, millimeter waves, characteristic impedance, attenuation constant, transition, 5G.

I. INTRODUCTION

To overcome the limited available amount of spectrum at microwave frequencies, millimeter-wave technology has been proposed to enable the future fifth-generation (5G) and beyond systems demanding high-data-rate access, such as high-data- rate wireless communications and automotive radar systems. Unfortunately, the conventional metal hollow waveguides can no longer realize efficient feeding networks for antenna arrays at the millimeter-wave band due to the small hole, which makes the manufacturing very challenging [1]. The gap waveguide (GW) is promising for the millimeter-wave applications, as no conducting joint is required between the artificial magnetic conductor (AMC) and the perfect electric conductor (PEC), both of which compose the waveguide [2]. However, the small periodic structures realizing the AMC at high frequencies still cause machining issues that we may have to return to the high-cost micro-electro-mechanical system (MEMS) process [3]. To address these problems, the microstrip-ridge GW and inverted- microstrip GW were proposed with the low-cost PCB process [4], [5]. However, the former suffers from the issues of plated vias in the conducting strip and the high-loss electroless nickel immersion gold (ENIG) coating, which cause large attenuation and a frequency shift [6]. While, it is very difficult for the later to be connected with planar lines or active components, which is also found in other GWs and metal waveguides mentioned above [7]–[11]. For example, as presented in [7] and [8], the microstrip-ridge GW (or, the inverted-microstrip GW) and the microstrip line were separately fabricated at different substrates, and their connection was realized through a pressure contact between the two substrates. Obviously, the transition efficiency and components reliability cannot be guaranteed, in addition to the design and fabrication complexities.

Recently, substrate integrated gap waveguide (SIGW) has been proposed to overcome the above-mentioned weaknesses in all of the current GWs [12]. Different from substrate integrated waveguide (SIW) of fundamental TE_{10} mode, as a quasi-TEM line, the SIGW has no mode conversion loss when integrating with microstrip lines or other TEM lines. And, the SIGW also allows us to design circuits and

The associate editor coordinating the review of this manuscript and approving it for publication was Nagendra Prasad Pathak.

components in the same way as microstrip line does, instead of the waveguide procedures as we used in the SIW. Taking these advantages, the SIGW has been employed to realize many cost-efficient components, such as wideband coupler and combiner for 5G applications [13], [14], bandpass filter [15], magneto-electric dipoles [16], [17], and slot antenna arrays [18], [19]. However, current designs of SIGW or other GWs have to use the very time-consuming full-wave and optimization simulation tools. This is because of their complex structures that cause very complicated closed-form and analytic expressions [20]–[23]. The empirical formulas reported recently in [24] based on non-linear curve fitting still get themselves in trouble of complexities and calculation errors, which can be even over 30% compared to the full-wave solutions.

In this work, we propose an approximate, but very convenient and accurate, manner to find the desired strip width for SIGW with a given characteristic impedance, including calculations of conductor and dielectric attenuation constants. With the help of our manner, no complex manual calculations or time-consuming full-wave simulation iterations will be required. Moreover, we will present that no additional transition structures, such as a microstrip taper, will be required for the SIGW to be integrated with microstrip lines at millimeter-wave bands. Both of the above works will be of great help to make our future designs much simpler and faster, such as feeding networks for SIGW antenna arrays or other types of cost-effective SIGW passive components at high frequencies.

II. DISPERSION CHARACTERISTIC OF SIGW

Fig. 1 is the dispersion diagram for one SIGW unit cell with a conducting strip, computed from the HFSS eigenmode solver. The strip with a width of 0.5 mm is grounded by the plated via. The fill-in substrate is Rogers RT/Duroid 6002 with ε_r of 2.94 and loss tan δ of 0.0012. The change of the SIGW fundamental mode, a quasi-TEM mode, with different substrates for the via- and gap-layers is revealed in Fig. 1 (c). As indicated by the solid red curve in Fig. 1 (c), even if the via-layer ε_r is fixed at 5 that is the same as in the case of dotted-dashed blue curve, the gap-layer ε_r decreasing from 5 to 3 makes the fundamental mode get more close to the dashed green curve for the via- and gap-layers with the same $\varepsilon_r = 3$. The same observation can be found in the dotted-dotted black curve when the gap-layer ε_r is increased to 10. This is important to let us know as the waves are mostly concentrated in the gap-layer, the characteristic impedance and line loss of the SIGW will be mainly determined by this layer substrate. While, the observed deviations between the solid red and dashed green curves or between the dotted-dotted black and dotted-dotted-dashed yellow curves reveals that the via-layer substrate may still have a limited effect on the SIGW characteristic. This is because that part of the fringing fields leaks into the via-layer due to the non-ideal AMC plane, which we should take into consideration for a more accurate design.

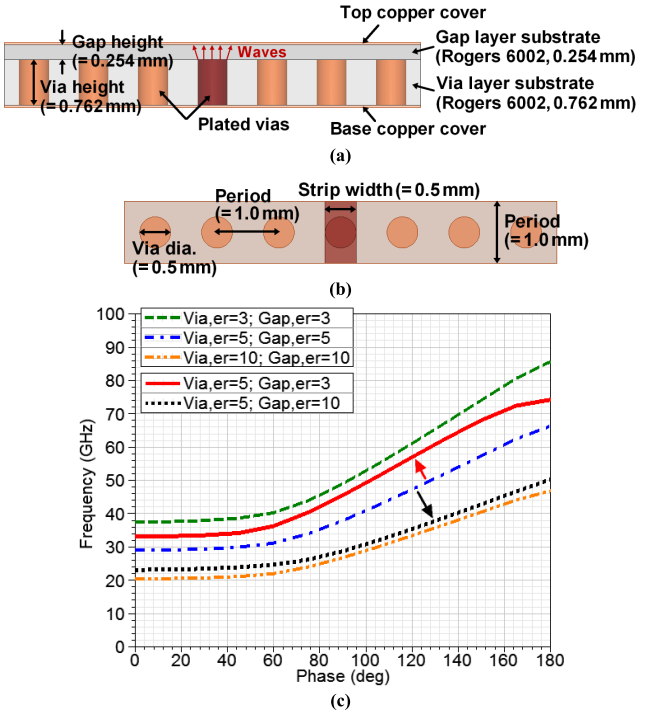

FIGURE 1. SIGW unit cell and dispersion characteristic. (a) Side view. (b) Top view. (c) Change in SIGW quasi-TEM modes with different substrates for the via- and gap-layers. Via-layer $\varepsilon_r = 5$, and gap-layer $\varepsilon_r = 3$ or 10. For comparison, the via- and gap-layers of the same substrate is also shown, i.e., $\varepsilon_r = 3$, 5, or 10.

III. MODELING AND EMPIRICAL FORMULAS

A. DESIGN OF CHARACTERISTIC IMPEDANCE

An SIGW based on the unit cell given in Fig. 1 is shown in Fig. 2 (a) with the same substrate, Rogers RT/Duroid 6002 for the gap- and via-layers. The simulated S_{21} and S_{11} are shown in Fig. 2 (b) with a passband from around 43 to 76 GHz. As found in [20], [25], and [26], the characteristic impedance of GW can be ideally calculated by a half-stripline model under an ideal AMC, which is twice the characteristic impedance of a stripline, $Z_{\text{stripline}}$, i.e.,

$$Z_{\text{gap waveguide}} = 2Z_{\text{stripline}}, \tag{1}$$

The ideal impedances from (1) for $\varepsilon_r = 3$, 5, and 10 are presented by three dotted-dotted black lines in Fig. 3. It can be also found from Fig. 3 that the real characteristic impedances of the SIGW, Z_{SIGW}, from the full-wave solutions, HFSS, are generally around 15-20 Ω lower than the ideal ones at the center frequencies of the passbands. As designing SIGW circuits, one usually needs to find the strip width given the characteristic impedance. Therefore, to achieve a more precise and practical design manner, a correction factor, Δ, is introduced in (1) to minimize their discrepancy, and thus (1) is changed to

$$Z_{\text{gap waveguide}} = 2Z_{\text{stripline}} - \Delta, \tag{2}$$

where Δ is chosen from 15 to 20 Ω. It is important to note that this correction range is very accurate, which we can also find in [20], [25], and [26].

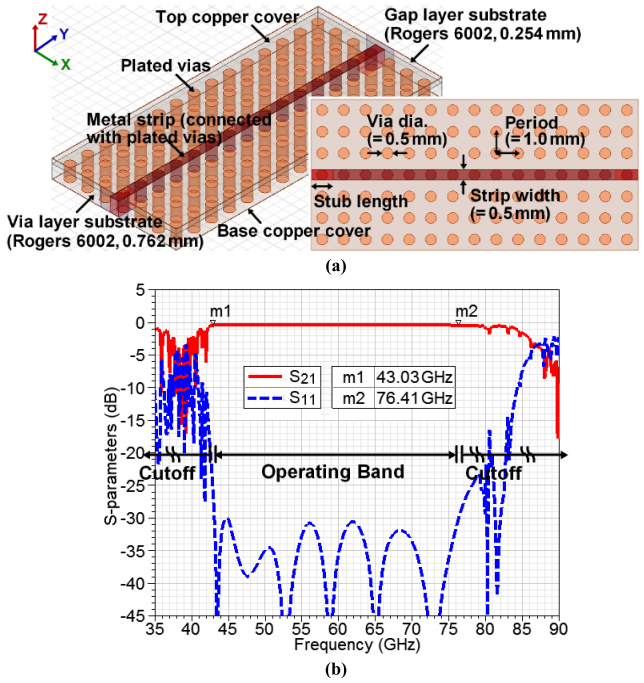

FIGURE 2. (a) Overview and top view of SIGW transmission model in simulations. (b) SIGW simulated transmission performance.

Consequently, to get the desired strip width of a 50 Ω SIGW with $\varepsilon_r = 3$, indicated by the solid red curve in Fig. 3, we can easily turn to work on the width of a stripline with $Z_{\text{stripline}}$ of 35 Ω (using $\Delta = 20\ \Omega$), i.e.,

$$Z_{\text{stripline}} = (Z_{\text{SIGW}} + \Delta)/2 = (50 + 20)/2\Omega = 35\Omega. \quad (3)$$

As provided in [27], the strip width, W, and the substrate thickness, h, of the stripline are related to each other by

$$\frac{W}{h} = \begin{cases} x & \text{for} \sqrt{\varepsilon_r} Z_{\text{stripline}} > 120\ \Omega \\ 0.85 - \sqrt{0.6 - x} & \text{for} \sqrt{\varepsilon_r} Z_{\text{stripline}} < 120\ \Omega, \end{cases} \quad (4)$$

where

$$x = \frac{30\pi}{\sqrt{\varepsilon_r} Z_{\text{stripline}}} - 0.441 \quad (5)$$

For the used substrate $\sqrt{\varepsilon_r} Z_{\text{stripline}} = \sqrt{2.94} \times 35 = 60.01 < 120$ and $x = 30\pi/(\sqrt{\varepsilon_r} Z_{\text{stripline}}) - 0.441 = 1.13$, (4) gives us the strip width as $W = hx = (2 \times 0.254)(1.13) = 0.57$ mm, which is very close to the full-wave solution of 0.5 mm.

It is important to note that the applied substrate thickness, h, in (4) is twice the thickness of the gap-layer substrate of 0.254 mm. Obviously, 0.57 mm is a very good initial value to start the full-wave optimization. Thanks to kinds of commercial software or free online calculation tools, such as LineCalc in ADS and Polar SI9000, the width of a stripline for a given characteristic impedance from (3) can be easily got, without any complicated or time-consuming manual calculations. Also, Fig. 3 offers us a simple guideline on how to choose a proper correction value, Δ. For example, if an SIGW with lower substrate ε_r, such as 3, it is better to choose a larger Δ (20 Ω for example); while a smaller Δ (15 Ω for example)

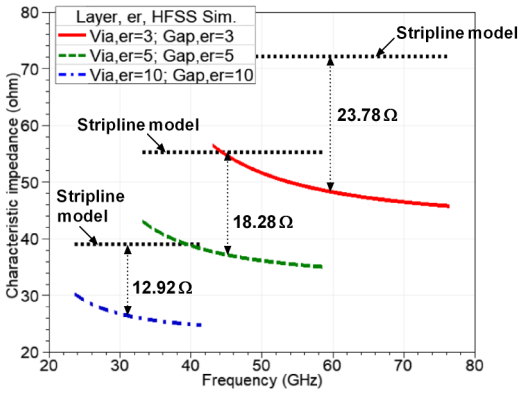

FIGURE 3. Comparisons between the SIGW characteristic impedances calculated from HFSS and conventional half-stripline model, considering the via- and gap-layers with the same substrate $\varepsilon_r = 3$, 5, or 10.

is more suitable for an SIGW with higher ε_r, as indicated by the dotted-dashed blue curve with ε_r of 10.

B. VIA- AND GAP-LAYERS OF DIFFERENT SUBSTRATES

As explained previously, part of the power may leak into the via-layer substrate and hence the SIGW impedance is affected. This effect is going to be investigated in this section, considering the gap- and via-layers of the SIGW in Fig. 2 with different dielectric substrates. A guideline of how to choose a proper correction factor, Δ, is finally given under this condition.

As illustrated by the dashed green curve in Fig. 4 (a), when the via-layer ε_r (= 5) is higher than the gap-layer ε_r (= 3), the SIGW characteristic impedance, Z_{SIGW}, is lowered by around 4 Ω at the center frequency. This means that the via-layer with larger ε_r has an effect of increasing the synthetic effective ε_r of the structure. Therefore, we can apply a larger Δ, such as 24 Ω, in (3), instead of 20 Ω used previously. In contrast, such a post-tuning of the correction factor, Δ, is smaller when the gap-layer with relatively larger ε_r, such as 5, as found in Fig. 4 (b). The decrease in Z_{SIGW} at the center frequency is only 2 Ω (instead of 4 Ω mentioned above), when the via-layer ε_r is increased from 5 to 7, as shown by the dashed green curve.

To help easily use the guidelines shown above, the proposed design manner is therefore summarized below, considering the gap- and via-layers using the same or different substrates.

1) For a given SIGW characteristic impedance, Z_{SIGW}, such as 50 or 75 Ω, the proposed simple formula (3) is used to have the corresponding stripline characteristic impedance $Z_{\text{stripline}}$, with a proper correction factor, Δ, ranging from 15 to 20 Ω.
2) When the via- and gap-layers of the SIGW using the same substrate, a large Δ (20 Ω for example) is suitable for the substrate with a small ε_r, such as 3 or 5. In contrast, a small Δ (15 Ω for example) should be adopted if the substrate has relatively large ε_r, 10, for example.

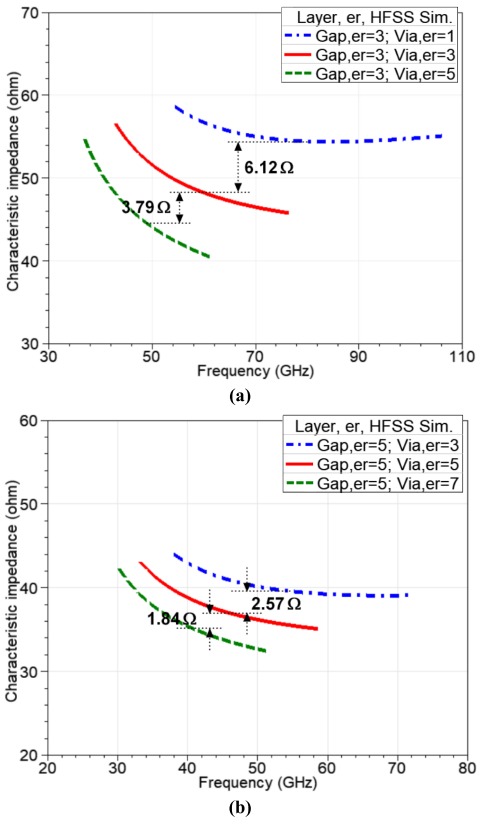

FIGURE 4. Simulated change in SIGW characteristic impedance with different substrates for the via- and gap-layers. (a) Gap-layer $\varepsilon_r = 3$, and via-layer $\varepsilon_r = 1$, 3, or 5. (b) Gap-layer $\varepsilon_r = 5$, and via-layer $\varepsilon_r = 3$, 5, or 7.

3) For the via- and gap-layers using different substrates, a proper value of Δ can be basically determined by the gap-layer substrate ε_r. For example, when the via-layer ε_r (= 5) is higher than the gap-layer ε_r (= 3), a larger Δ (24 Ω for example) is more accurate, substituting for 20 Ω in step 2), due to the increased synthetic effective ε_r (between 3 and 5). Such a post-tuning range is smaller when the gap-layer with larger ε_r, such as 5 or 10, and only 2 Ω or less is needed in this post-tuning for the Δ got in step 2).
4) After finding a proper Δ, commercial or online calculation tools can be used to quickly compute the strip width of a stripline for a given $Z_{\text{stripline}}$ from step 1). This is the initial width for our desired SIGW with a high degree of accuracy compared to the full-wave solution.

C. CALCULATAION OF ATTENUATION CONSTANTS

In this part, we will study the effect of loss on transmission line behavior and show how the attenuation constant for dielectric and conductor losses can also be calculated using the above proposed manner, which will also be proven by the full-wave solution. As provided in [27], the dielectric attenuation of a stripline can be calculated by

$$\alpha_d = \frac{k \tan \delta}{2}, \tag{6}$$

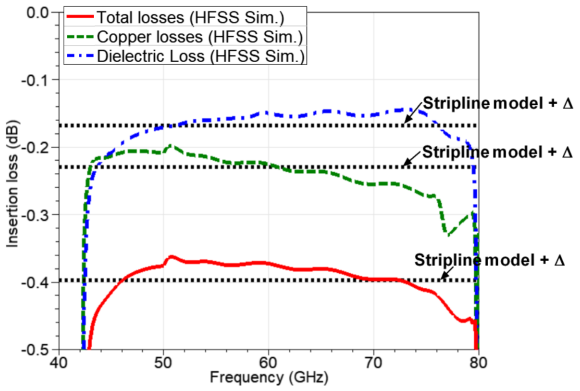

FIGURE 5. Comparison of different types of SIGW insertion loss, along with the impedances calculated from the proposed modified stripline model presented by the dotted-dotted black lines.

where $k = 2\pi f\sqrt{\varepsilon_r}/c$ is the wave number, f is the frequency, and c is the speed of light in free-space. Considering the SIGW given in Fig. 3 with ε_r of 2.94 and tan δ of 0.0012, the wave number and dielectric loss at the center frequency of 60 GHz are $k = 2154.68m^{-1}$ and $\alpha_d = 1.29Np/m = 11.23dB/m$. The total dielectric loss for this SIGW of 15 mm length are then (11.23)(0.015) = 0.17 dB, which has been presented in Fig. 5 and show good agreement with the full-wave solution (dotted-dotted black line, from HFSS) over a broad band.

Correspondingly, the attenuation constant for conductor loss of the stripline is as follows [27].

$$\alpha_c = \begin{cases} \dfrac{2.7\times10^{-3}R_s\varepsilon_r Z_{stripline}}{30\pi(h-t)}A & \text{for } \sqrt{\varepsilon_r}Z_{\text{stripline}} < 120\Omega \\ \dfrac{0.16R_s}{Z_0 h}B & \text{for } \sqrt{\varepsilon_r}Z_{\text{stripline}} < 120\Omega \end{cases} \tag{7}$$

with

$$A = 1 + \frac{2W}{h-t} + \frac{1}{\pi}\frac{h+t}{h-t}\ln\left(\frac{2h-t}{t}\right),$$

$$B = 1 + \frac{h}{(0.5W+0.7t)}\left(0.5 + \frac{0.414t}{W} + \frac{1}{2\pi}\ln\frac{4\pi W}{t}\right),$$

where h is the thickness of the substrate (twice the gap-layer thickness as explained previously), W and t is the strip width and thickness, respectively. Considering the previous case of $Z_{\text{SIGW}} = 50\ \Omega$ and $\Delta = 20\ \Omega$, the stripline characteristic impedance, $Z_{\text{stripline}}$, used in (7) is 35 Ω. As $W = 0.57$ mm and $t = 0.018$ mm, $\sqrt{\varepsilon_r}Z_{stripline} = 60.01 < 120$ and $A = 4.71$, (7) gives the conductor attenuation as $\alpha_c = 1.82Np/m = 15.77$ dB/m. The surface resistance of copper, R_s, is 0.064 at 60 GHz [28]. The total conduction attenuation of this 15 mm length SIGW is then 0.24 dB, which also has excellent agreement with the full-wave solution shown by the dashed green curve in Fig. 5. It is also found that the conductor loss makes the main contribution to the total attenuation and may even increase with frequencies. The total attenuation constant can be then obtained by

$$\alpha = \alpha_d + \alpha_c = 3.11\text{Np/m} = 27\ \text{dB/m}, \tag{8}$$

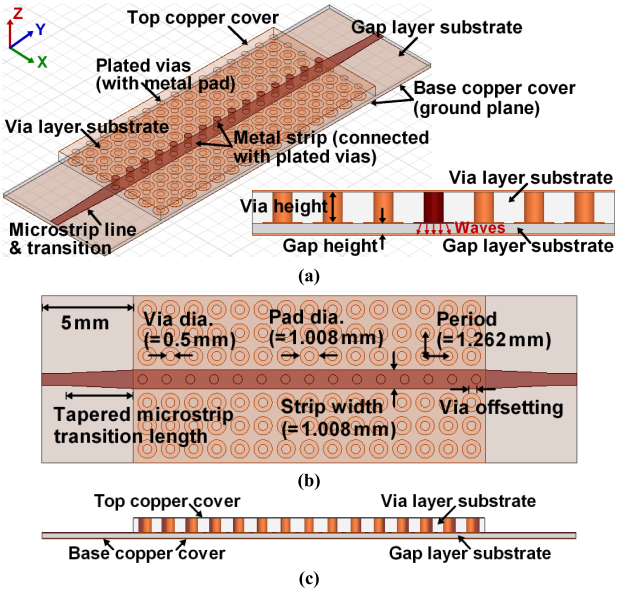

FIGURE 6. SIGW with transitions to microstrip lines. (a) Overview and front/back view. (b) Top view. (c) Side view.

which gives a total insertion loss of 0.41 dB for a 15 mm length and is proven by the full-wave solution indicated by the solid red curve in Fig. 5.

Still, the works of (6) - (8) can be conveniently done by using LineCalc in ADS, Polar SI9000, or other free online calculation tools, without any manual computations. Therefore, in addition to helping find the desired strip width for SIGW with a given characteristic impedance, the proposed empirical formulas are also very convenient and accurate to predict the loss performance. Obviously, this will significantly improve our designs and make them much easier and faster, without any complex calculations by hand or time-consuming iterations of full-wave simulations.

IV. TRANSITION BETWEEN SIGW AND MICROSTRIP LINE

The SIGW with a conventional tapered microstrip transition is shown in Fig. 6. As fabricated with PCB technology, a metal pad is attached to the plated via end for its metalized process. The space between the hole edge and copper edge is 0.254 mm and thus the diameter of the pad is 1.008 mm. The period is then enlarged to 1.262 mm to separate the adjacent pads sufficiently, and the strip width is increased to 1.008 mm as well. The lower gap-layer substrate is Rogers RT/Duroid 6002 of 0.254 mm thickness, and it is 5 mm longer than the upper via-layer at the input and output, respectively, to place the microstrip feed line. The via-layer realizing the AMC surface has two cases: Rogers RT/Duroid 6002 of 0.762 mm thickness, and Rogers RT/Duroid 6006 of 0.635 mm thickness ($\varepsilon_r = 6.15$ and $\tan\delta = 0.0027$). They are corresponding to the above study that the via- and gap-layers are made of the same or different substrates. It is seen from Fig. 7 that different via-layer substrates create two different passbands, which are from around 27 to 57 GHz and from around 25.4 to 48.8 GHz, respectively.

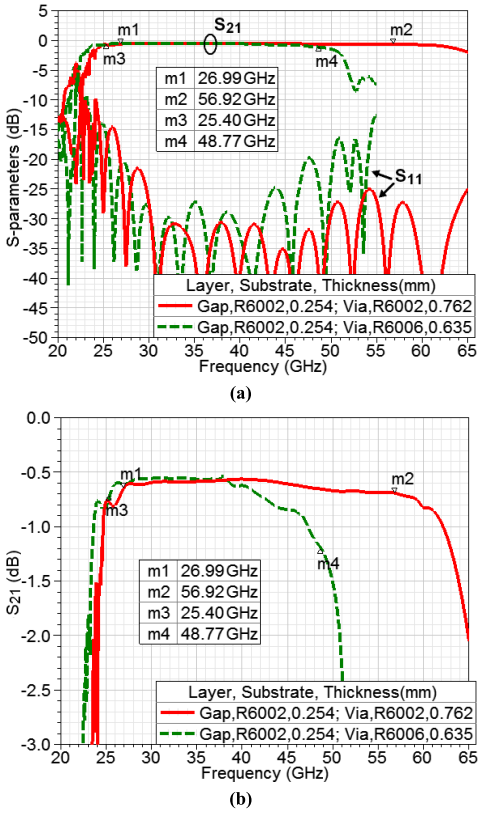

FIGURE 7. Simulated performance of the tapered microstrip transitions for the SIGW with the same or different substrates for the gap and via layers. (a) S_{11} and S_{21}. (b) Zoom-in S_{21}.

The width of the 50 Ω microstrip feed lines for the above two passbands is almost the same, which is around 0.64 mm at the passband center frequency. To achieve the desired transmission performance with minimized return loss, S_{11}, over the band, the length of the tapered microstrip transitions has to be optimized, which is 4.05 and 3.9 mm for the via-layer substrate of Rogers RT/Duroid 6002 and 6006, respectively. Fig. 7 (a) presents that good transition performance is obtained over a broad band with the designed microstrip tapers. While, compared to the solid red curve, the increased S_{11} is found in the dashed green curve at the high frequencies. This can be explained by the dashed green curve in Fig. 4 (a) that the via-layer with ε_r higher than the gap- layer ε_r will degrade impedance flatness over a broad band. The microstrip taper cannot offer such a broadband transition, while other transition structures could be helpful, such as an exponential taper [27].

To get good transmission performance, the above constructed transition in Fig. 6 has to use microstrip tapered lines, with an additional offsetting of the plated vias attached in the strip. This is because that the enlarged period and strip width as well as the used copper pad due to the PCB process lower the characteristic impedance of the originally designed SIGW in Fig. 2 of 0.5 mm width. The resulting Z_{SIGW} is smaller than 40 Ω over most of the passband, rather than our desired 50 Ω. Therefore, if the SIGW

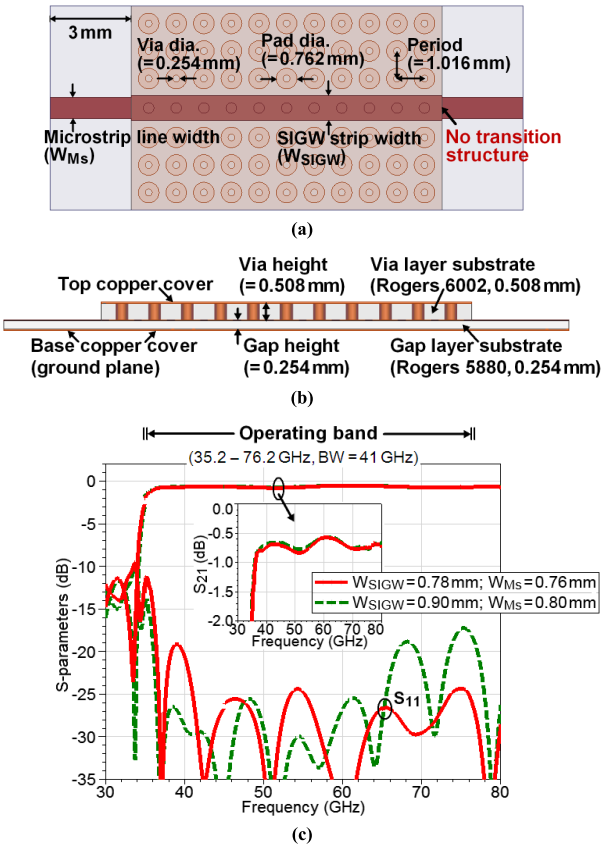

FIGURE 8. SIGW without additional external transition to the microstrip line. (a) Top view of the circuit. (b) Side view of the circuit. (c) Simulated S_{11} and S_{21}.

can be correctly designed under the PCB technology with Z_{SIGW} of 50 Ω, the additional microstrip taper would be minimized or removed totally for the desired transmission performance.

An SIGW without any transition structure set at the input or output is shown in Fig. 8 (a). The simulated results are given in Fig. 8 (c), considering two cases. One SIGW has a strip width of 0.9 mm that offers a characteristic impedance of 50 Ω at the center frequency of the passband of 55.7 GHz. The other has a strip width of 0.78 mm, giving a characteristic impedance of 55 Ω at 55.7 GHz. It is found that by combining with a proper width of the microstrip feed line, it is achievable to obtain the desired transmission performance over a broad band. In particular, the former of 0.9 mm strip width is better at the middle band as shown by the dashed green curve; while the one of 0.78 mm strip width plays better at the higher bands. The microstrip line of 0.76 mm width has a characteristic impedance of 50 Ω at 55.7 GHz. Obviously, as with the same fundamental mode, a quasi-TEM mode, and sharing the same guiding strip, ground, and substrate, these two types of transmission lines have almost the same strip width under the same Z_0, and thus no transition structures are required any more. This will be of great help to make our future designs and structures much faster and more compact.

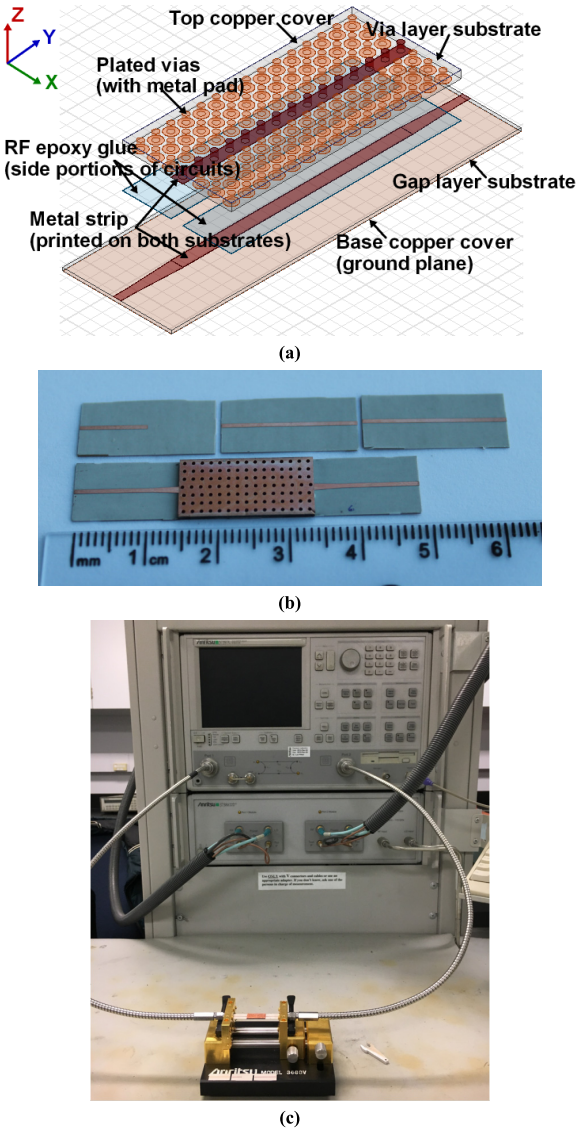

FIGURE 9. (a) Distributed 3-D view of the fabrication for the designed SIGW. (b) Photo of the fabricated SIGW with the tapered microstrip transitions, including TRL calibration kits. (c) Photo of the measurement set-up.

V. EXPERIMENTAL VERIFICATION AND ANALYSIS

The two SIGWs shown above with or without a microstrip taper transition have been fabricated, as presented in Figs. 9 and 11, respectively. The former with a microstrip taper is the one given in Fig. 6 using Rogers RT/Duroid 6002 and 6006 for the gap- and via-layers, respectively. And, the other without transition is the one in Fig. 8, with 0.78 and 0.76 mm width for the SIGW strip and microstrip line, respectively. As illustrated in Fig. 9 (a), the plated via in the top-layer substrate and the metal strips on both layers are first processed, and then the two substrates are stuck together using a thin layer RF glue, with high pressure and temperature. In the fabrication, the glue is located only in the side portions of the circuits. As the glue thickness is only 5 μm, much thinner than the copper thickness of 18 μm, a tight electrical contact between the two printed strips can be ensured. Moreover,

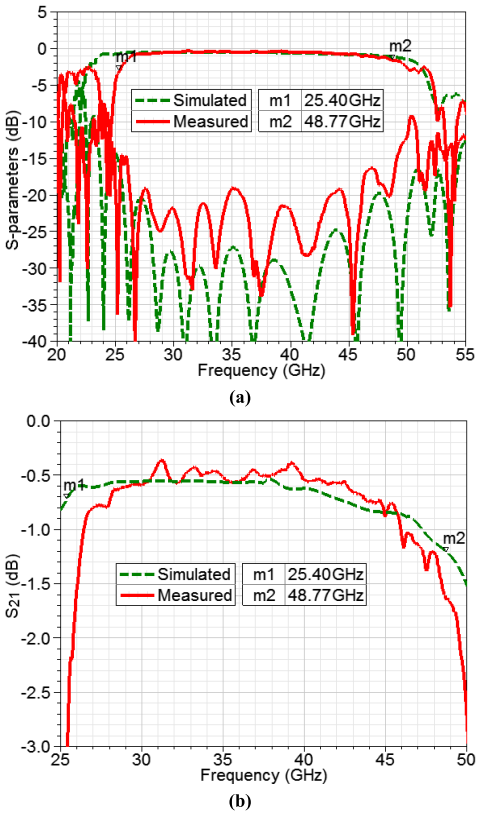

FIGURE 10. Measured *S*-parameters of the fabricated SIGW, compared with the simulated. (a) S_{11} and S_{21}. (b) Zoom-in S_{21}.

it can be found that as the waves travel under the lower surface of the lower strip, they will no longer interact with the plated vias (only in the upper strip) or the high-loss ENIG coating (only on the copper outer surface). Therefore, the possible substantial losses or frequency shifts due to the vias in the strip and the ENIG coating will no longer occur in SIGW, compared to the microstrip-ridge GW or the inverted-microstrip GW mentioned previously. In addition, stable gap performance is now guaranteed by the gap-layer substrate, rather than the unstable air gap existing in all current GWs. This is significant as maintaining a constant air gap height over a large circuit is very challenging, in particular in large antenna arrays.

The Thru-Reflect-Line (TRL) calibration kits used in tests to remove the effect of the test fixture are also shown in Fig. 9 (b), including: 1) a thru of 20 mm length; 2) an open circuit with a microstrip of 10 mm length, i.e., half-length of the thru; and 3) a line which is 1.297 mm longer than the thru, corresponding to a quarter wavelength at 37 GHz. The substrate of the kit circuits is Rogers RT/Duroid 6002 of 0.254 mm thickness, the same as the bottom substrate of this fabricated SIGW prototype. The measured S_{21} and S_{11} from a vector network analyzer (VNA) are shown in Fig. 10, which have clear and good agreement with the simulated, in both the achieved passband and the in-band performance. The TRL calibration kits for the other SIGW prototype without the transition can also be found in Fig. 11 (a), which

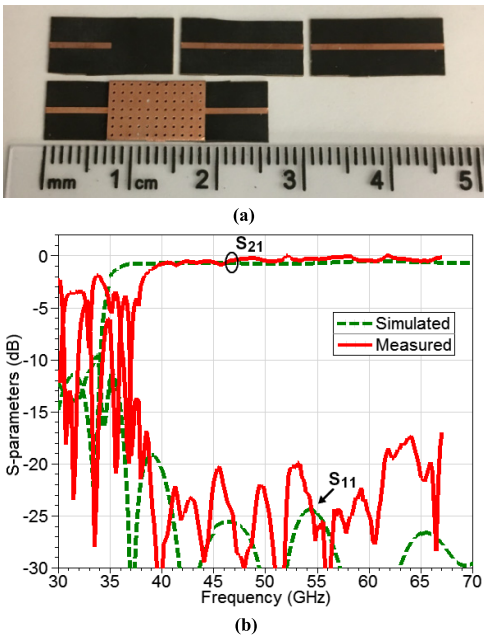

FIGURE 11. (a) Photo of the fabricated SIGW without additional external transition to microstrip lines ($W_{SIGW} = 0.78$ mm and $W_{MS} = 0.76$ mm), including TRL calibration kits. (b) Measured and simulated S_{11} and S_{21}.

contains 1) a thru of 15 mm length; 2) an open circuit with a microstrip of 7.5 mm length, i.e., half-length of the thru; and 3) a line that is 1.115 mm longer than the thru, equal to a quarter wavelength at 48.5 GHz. They use the same substrate as the gap-layer of this SIGW prototype, i.e., Rogers RT/Duroid 5880 of 0.254 mm thickness. The measured *S*-parameters given in Fig. 11 (b) also show good agreement with the simulation performance. Moreover, it can be seen that the measured S_{21} and S_{11} are at the same level of the measured performance of the SIGW with a microstrip taper transition shown in Fig. 10, which validates our design. Due to the available test frequency of the test fixture and VNA, the measurements are only up to 67 GHz. The deviations between the measured and simulated results could be due to the used glue, the deformation of the too soft bottom substrate, the fabrication tolerance, or the substrate frequency-dependent ε_r and tan δ, which were not considered in simulations.

The measured transition performance of the SIGW with or without a microstrip taper is compared with other reported works in Table 1, in terms of transition technique, fractional bandwidth, and return loss. It is evident that the SIGW may have the better bandwidth and in-band return loss than other GW versions, when integrating with the microstrip line, even if without any transition structure. In contrast, as explained previously, the transition simply using a pressure contact will cause reliability issues and cannot get in future mass production. While, the other transition techniques as presented in [9], [10], [29], and [30] will obviously cause an increase in the design complexity and manufacturing cost, and may still cannot get the desired performance compared to the SIGW.

TABLE 1. Comparisons of measured GW transition performance.

Ref.	GW type	Feeding type	Transition technique	Fractional bandwidth (%)	Return loss (dB)
[7]	Microstrip-ridge GW	Microstrip	Pressure contact	38.5% (23.7-35.0 GHz)	15 (Sim.)
[8]	Inv. microstrip GW	Microstrip	Pressure contact	39.3% (21.5-32.0 GHz)	20 (Sim.)
[9]	Inv. microstrip GW	WR15	E-plane probe	21.5% (57.0-70.7 GHz)	10
[10]	Metal-ridge GW	Microstrip	Defected ground slot	45.8% (11.8-18.8 GHz)	10
[11]	Metal-ridge GW	Microstrip	Pressure contact	60.6% (23.0-43.0 GHz)	14
[29]	Microstrip-ridge GW	Coaxial	Matching section and vias	46.1% (25.0-40.0 GHz)	10
[30]	Microstrip-ridge GW	Microstrip	SIW bridge	31.5% (75-103 GHz)	10
This work	SIGW	Microstrip	Microstrip taper	62.7% (25.5-48.8 GHz)	15
This work	SIGW	Microstrip	None	64.3% (39.0-76.0 GHz)	17

VI. CONCLUSION

An approximate, but very convenient and accurate, manner is proposed to help find the desired strip width for SIGW with a given characteristic impedance and the conductor and dielectric attenuation constants, without any complex manual calculations or time-consuming iterations of full-wave simulations. A clear guideline has also been offered for how to perform this simple method. Moreover, we have verified that no additional transition structure, such as a conventional microstrip taper, is required any more for the SIGW to be integrated with microstrip lines, for the desired transmission performance. This will further help realize a fast and simple design. Both of the above works are proven by full-wave simulations and experimental tests, and will be of great help to realize future feeing networks for SIGW antenna arrays or other types of cost-effective SIGW passive components at high frequencies. It is worth noticing that, although the above proposed design manner is derived based on SIGW, it could be extended to other GW versions, the microstrip-ridge GW and the inverted-microstrip GW, for example.

ACKNOWLEDGMENT

The authors express their gratitude to T. Antonescu, with the Poly-Grames Research Center, École Polytechnique de Montreal, Montreal, QC, Canada, for his technical assistance in the fabrication of the experimental prototypes. They would also like to thank the Editors and the anonymous reviewers for their insightful comments and constructive suggestions.

REFERENCES

[1] P.-S. Kildal, A. U. Zaman, E. Rajo-Iglesias, E. Alfonso, and A. Valero-Nogueira, "Design and experimental verification of ridge gap waveguide in bed of nails for parallel-plate mode suppression," *IET Microw., Antennas Propag.*, vol. 5, no. 3, pp. 262–270, Mar. 2011.

[2] P.-S. Kildal, E. Alfonso, A. Valero-Nogueira, and E. Rajo-Iglesias, "Local metamaterial-based waveguides in gaps between parallel metal plates," *IEEE Antennas Wireless Propag. Lett.*, vol. 8, no. 4, pp. 84–87, Apr. 2009.

[3] S. Rahiminejad, A. U. Zaman, E. Pucci, H. Raza, V. Vassilev, S. Haasl, P. Lundgren, P.-S. Kildal, and P. Enoksson, "Micromachined ridge gap waveguide and resonator for millimeter-wave applications," *Sens. Actuators A, Phys.*, vol. 186, pp. 264–269, Oct. 2012.

[4] H. Raza, J. Yang, P.-S. Kildal, and E. A. Alós, "Microstrip-ridge gap waveguide–study of losses, bends, and transition to WR-15," *IEEE Trans. Microw. Theory Techn.*, vol. 62, no. 9, pp. 1943–1952, Sep. 2014.

[5] E. Pucci, E. Rajo-Iglesias, J. L. Vázquez-Roy, and P.-S. Kildal, "Planar dual-mode horn array with corporate-feed network in inverted microstrip gap waveguide," *IEEE Trans. Antennas Propag.*, vol. 62, no. 7, pp. 3534–3542, Jul. 2014.

[6] S. A. Razavi, P.-S. Kildal, L. Xiang, E. A. Alós, and H. Chen, "2× 2-Slot element for 60-GHz planar array antenna realized on two doubled-sided PCBs using SIW cavity and EBG-type soft surface fed by microstrip-ridge gap waveguide," *IEEE Trans. Antennas Propag.*, vol. 62, no. 9, pp. 4564–4573, Sep. 2014.

[7] M. S. Sorkherizi and A. A. Kishk, "Self-packaged, low-loss, planar bandpass filters for millimeter-wave application based on printed gap waveguide technology," *IEEE Trans. Compon., Packag., Manuf. Technol.*, vol. 7, no. 9, pp. 1419–1431, Sep. 2017.

[8] E. Rajo-Iglesias and A. A. Brazález, "5G antenna in inverted microstrip gap waveguide technology including a transition to microstrip," in *Proc. Int. Symp. Antennas Propag.*, Okinawa, Japan, Oct. 2016, pp. 1042–1043.

[9] A. A. Brazález, E. Rajo-Iglesias, J. L. Vázquez-Roy, A. Vosoogh, and P.-S. Kildal, "Design and validation of microstrip gap waveguides and their transitions to rectangular waveguide, for millimeter-wave applications," *IEEE Trans. Microw. Theory Techn.*, vol. 63, no. 12, pp. 4035–4050, Dec. 2015.

[10] B. Molaei and A. Khaleghi, "A novel wideband microstrip line to ridge gap waveguide transition using defected ground slot," *IEEE Microw. Wireless Compon. Lett.*, vol. 25, no. 2, pp. 91–93, Feb. 2015.

[11] A. U. Zaman, T. Vukusic, M. Alexanderson, and P.-S. Kildal, "Design of a simple transition from microstrip to ridge gap waveguide suited for MMIC and antenna integration," *IEEE Antennas Wireless Propag. Lett.*, vol. 12, pp. 1558–1561, 2013.

[12] J. Zhang, X. Zhang, and D. Shen, "Design of substrate integrated gap waveguide," in *IEEE MTT-S Int. Microw. Symp. Dig.*, San Francisco, CA, USA, May 2016, pp. 1–4.

[13] D. Shen, K. Wang, and X. Zhang, "A substrate integrated gap waveguide based wideband 3-dB coupler for 5G applications," *IEEE Access*, vol. 6, pp. 66798–66806, 2018.

[14] K. Eslami and K. Afrooz, "Rat-race power divider/combiner for 5G application using substrate integrated gap waveguide," in *Proc. 5th Int. Conf. Millim.-Wave THz Technol.*, Tehran, Iran, Dec. 2018, pp. 101–104.

[15] M. Dong, D. Shen, X. Zhang, W. Ren, Z.-H. Ma, R. Qian, and H. Yuan, "Substrate integrated gap waveguide bandpass filters with high selectivity and wide stopband," in *IEEE MTT-S Int. Microw. Symp. Dig.*, Philadelphia, PA, USA, Jun. 2018, pp. 285–288.

[16] D. Shen, C. Ma, W. Ren, X. Zhang, Z. Ma, and R. Qian, "A low-profile substrate-integrated-gap-waveguide-fed magnetoelectric dipole," *IEEE Antennas Wireless Propag. Lett.*, vol. 17, no. 8, pp. 1373–1376, Aug. 2018.

[17] C. Ma, M. Dong, and D. Shen, "A printed magneto-electric dipole based on substrate integrated gap waveguide," in *Proc. 6th Asia–Pacific Conf. Antennas Propag.*, Xi'an, China, Oct. 2017, pp. 1–3.

[18] J. Zhang, X. Zhang, and A. A. Kishk, "Broadband 60 GHz antennas fed by substrate integrated gap waveguides," *IEEE Trans. Antennas Propag.*, vol. 66, no. 7, pp. 3261–3270, Jul. 2018.

[19] D. Shen, C. Ma, and X. Zhang, "Substrate integrated gap waveguide circularly polarized slot antenna," in *Proc. IEEE Asia–Pacific Conf. Antennas Propag.*, Auckland, New Zealand, Aug. 2018, pp. 460–461.

[20] A. Polemi and S. Maci, "Closed form expressions for the modal dispersion equations and for the characteristic impedance of a metamaterial-based gap waveguide," *IET Microw., Antennas Propag.*, vol. 4, no. 8, pp. 1073–1080, Aug. 2010.

[21] M. Bosiljevac, Z. Sipus, and P.-S. Kildal, "Construction of Green's functions of parallel plates with periodic texture with application to gap waveguides—A plane-wave spectral-domain approach," *IET Microw., Antennas Propag.*, vol. 4, no. 11, pp. 1799–1810, Nov. 2010.

[22] A. Polemi, S. Maci, and P.-S. Kildal, "Dispersion characteristics of a metamaterial-based parallel-plate ridge gap waveguide realized by bed of nails," *IEEE Trans. Antennas Propag.*, vol. 59, no. 3, pp. 904–913, Mar. 2011.
[23] M. Vukomanović, M. Bosiljevac, and Z. Šipuš, "Efficient analysis of gap-waveguide structures through a rigorous mode-matching approach," in *Proc. ELMAR*, Zadar, Croatia, Sep. 2014, pp. 1–4.
[24] A. T. Hassan, M. A. M. Hassan, and A. A. Kishk, "Modeling and design empirical formulas of microstrip ridge gap waveguide," *IEEE Access*, vol. 6, pp. 51002–51010, 2018.
[25] E. Alfonso, P.-S. Kildal, M. Baquero, and A. Valero-Nogueira, "Study of the characteristic impedance of a ridge gap waveguide," in *Proc. IEEE Antennas Propag. Soc. Int. Symp.*, Charleston, SC, USA, Jun. 2009, pp. 1–4.
[26] H. Raza, J. Yang, P.-S. Kildal, and E. Alfonso, "Resemblance between gap waveguides and hollow waveguides," *IET Microw., Antennas Propag.*, vol. 7, no. 15, pp. 1221–1227, 2013.
[27] D. M. Pozar, *Microwave Engineering*. New York, NY, USA: Wiley, 2011.
[28] M. P. Kirley and J. H. Booske, "Surface resistance of copper from 400 to 850 GHz," in *Proc. IEEE 14th Int. Vac. Electron. Conf.*, Paris, France, May 2013, pp. 1–2.
[29] I. Afifi, M. M. M. Ali, and A.-R. Sebak, "Analysis and design of a wideband coaxial transition to metal and printed ridge gap waveguide," *IEEE Access*, vol. 6, pp. 70698–70706, 2018.
[30] Y. Shi, W. Feng, H. Wang, W. Che, Q. Xue, J. Wang, J. Zhang, X. Qian, M. Zhou, and B. Cao, "Novel W-band LTCC transition from microstrip line to ridge gap waveguide and its application in 77/79 GHz antenna array," *IEEE Trans. Antennas Propag.*, vol. 67, no. 2, pp. 915–924, Feb. 2019.

JING ZHANG (S'09) received the bachelor's degree from Leshan Normal University, Leshan, China, in 2007, the master's degree from the University of Electronic Science and Technology of China, Chengdu, China, in 2010, and the Ph.D. degree from Concordia University, Montreal, QC, Canada, all in electrical engineering. His current research interests include novel low-loss millimeter-wave transmission lines and antenna arrays for 5G and beyond applications.

XIUPU ZHANG (M'00–SM'07) received the B.Sc. degree from the Harbin Institute of Electrical Technology, Harbin University of Science and Technology, Harbin, China, in 1983, the M.Sc. degree from the Beijing University of Posts and Telecommunications, Beijing, China, in 1988, and the Ph.D. degree from the Technical University of Denmark, Lyngby, Denmark, in 1996, all in electrical engineering.

From 1983 to 1985, he worked for manufacturing fibers and fiber cables in China. From 1988 to 1992, he was with the Construction of Telecommunication Networks, Beijing, China. In 1992, he spent approximately one and a half years with the Chalmers University of Technology, Gothenburg, Sweden, where he investigated high-speed fiber-optic transmission. From 1998 to 2002, he was a Senior Engineer, in the fiber-optics industry, involved in the design of repeaterless fiber-optic transmission systems, erbium-doped fiber amplifiers and fiber Raman amplifiers, optical transmitters and receivers, and metropolitan optical networks, at North America including Montreal and Ottawa, Canada, and Piscataway, NJ, USA. In June 2002, he joined Concordia University, Montreal, Quebec, Canada, and became an Associate Professor. He is currently a Full Professor with the Department of Electrical and Computer Engineering, Concordia University. He has authored and coauthored more than 200 refereed technical publications, including 130 journal publications published in the IEEE Optical Society of America, and other related journals, and approximately 100 conference presentations in the IEEE related conferences such as the Optical Fiber Communications Conference. His current research interests include broadband and high-linearity radio over fiber (RoF) fronthaul transmission systems, quantum-dot semiconductor lasers, and broadband photodiodes.

He serves as an Associate Editor for the IEEE PHOTONICS Journal and an Academic Editor for MDPI *Journal of Applied Sciences*.

AHMED A. KISHK (M'86–SM'90–F'98) is currently a Professor with Concordia University, Montreal, QC, Canada, and Tier 1 Canada Research Chair in Advanced Antenna Systems. He has authored or coauthored more than 310 refereed journal articles and 420 conference papers. He has coauthored four books and several book chapters and editor of a book. He conducted several short courses at international conferences. His current research interests include the design of dielectric resonator antennas, microstrip antennas, small antennas, microwave sensors, radio frequency identification antennas for readers and tags, multifunction antennas, microwave circuits, electromagnetic bandgap, artificial magnetic conductors, soft and hard surfaces, phased array antennas, and computer-aided design for antennas, the design of millimeter frequency antennas, and feeds for parabolic reflectors.

Dr. Kishk is a Fellow of the Electromagnetic Academy and the Applied Computational Electromagnetic Society. He was a recipient of many awards, including the Outstanding Paper Awards, in 1995 and 2006, for papers published in the *Applied Computational Electromagnetic Society Journal*, and the Microwave Theory and Techniques Society Microwave Prize, in 2004. He is an Editor of the *IEEE Antennas and Propagation Magazine*.